Phys Chem Minerals (2012) 39:515–523
DOI 10.1007/s00269-012-0507-y

ORIGINAL PAPER

Thermodynamic and magnetic properties of surface Fe^{3+} species on quartz: effects of gamma-ray irradiation and implications for aerosol–radiation interactions

Gobburu SivaRamaiah · Yuanming Pan

Received: 14 November 2011 / Accepted: 1 April 2012 / Published online: 24 April 2012

Abstract Samples of a natural amethyst, pulverized in air, and irradiated for gamma-ray doses from 0.14 to 70 kGy, have been investigated by powder electron paramagnetic resonance (EPR) spectroscopy from 90 to 294 K. The powder EPR spectra show that the surface Fe^{3+} species on the gamma-ray-irradiated quartz differ from its counterpart without irradiation in both the effective g value and the observed line shape, suggesting marked radiation effects. This suggestion is supported by quantitatively determined thermodynamic properties, magnetic susceptibility, relaxation times, and geometrical radius. In particular, the surface Fe^{3+} species on gamma-ray-irradiated quartz has larger Gibbs and activation energies than its non-irradiated counterpart, suggesting radiation-induced chemical reactions. The shorter phase-memory time (T_m) but longer spin–lattice relaxation time (T_1) of the surface Fe^{3+} species on the gamma-ray-irradiated quartz than that without irradiation indicate stronger dipolar interactions in the former. Moreover, the calculated geometrical radius of the surface Fe^{3+} species on the gamma-ray-irradiated quartz is three orders of magnitude larger than that of its counterpart on the as-is sample. These results provide new insights into radiation-induced aerosol nucleation, with relevance to atmospheric cloud formation and global climate changes.

G. SivaRamaiah · Y. Pan (✉)
Department of Geological Sciences,
University of Saskatchewan,
Saskatoon, SK S7N 5E2, Canada
e-mail: yuanming.pan@usask.ca

G. SivaRamaiah
Department of Physics,
Government College for Men,
Kadapa 516004, India

Keywords Quartz · Surface Fe^{3+} · Gamma-ray-radiation · EPR · Thermodynamic properties · Magnetic susceptibility · Mineral dust · Aerosol–radiation interactions

Introduction

Solid aerosol particles, including mineral dust, are important sources of air pollution and are known to exert profound impacts on global climate changes and biological processes (Lohmann and Feichter 2005; Andreae and Rosenfeld 2008; Buseck and Pósfai 2010). Quantitative understanding of the effects of solid aerosol particles on global climate changes require detailed data about their sources and physicochemical properties. However, knowledge about solid aerosol particles such as mineral dust, unlike their gaseous and liquid counterparts, remains limited (Buseck and Pósfai 2010). For example, solid aerosol particles in the atmosphere are known to experience prolonged exposure to and interactions with various cosmic radiations, including high-energy particles such as electrons, muons, and protons. However, dedicated studies on the effects of cosmic radiation on the bulk and surface properties of mineral dust are rare. In this context, the effects of radiation on surface species on quartz are particularly interesting, because it is one of the most common constituents in mineral dust (Claquin et al. 1999; Tatarov and Sugimoto 2005).

Our previous study of amethyst pulverized in air showed that its electron paramagnetic resonance (EPR) spectra are characterized by a broad peak at the effective $g = \sim 10.8$ (Fig. 1; SivaRamaiah et al. 2011). This peak does not correspond to any known lattice-bound Fe^{3+} centers in quartz (Barry and Moore 1964; Matarrese et al. 1969;

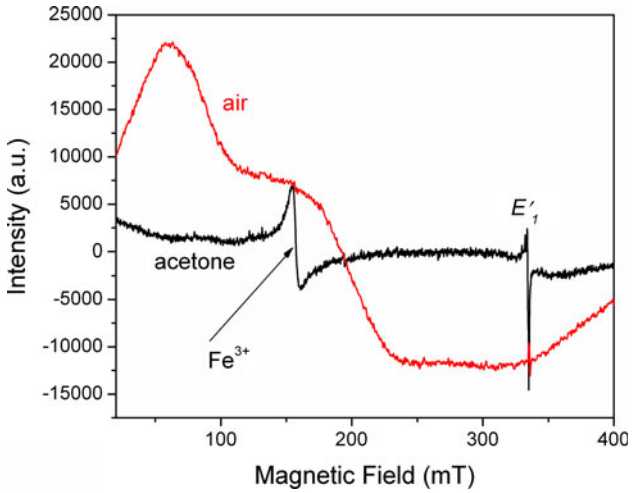

Fig. 1 Comparison of powder EPR spectra of a natural amethyst quartz pulverized in air (from SivaRamaiah et al. 2011) and in acetone, measured at 294 K and microwave frequencies of ~9.38 GHz. Note that the substitutional Fe^{3+} center at $g = \sim 4.28$ in the sample pulverized in acetone is marked

Mombourquette et al. 1986; Halliburton et al. 1989; Minge et al. 1989, 1990; Weil 1994; Balitsky et al. 2000; Di Benedetto et al. 2010) and was interpreted to represent surface Fe^{3+} species formed during sample preparation (SivaRamaiah et al. 2011). It is well known that Fe^{2+} is the dominant iron species in natural quartz and is expected to oxidize, migrate, and cluster to form surface Fe^{3+} species during pulverization in air (Cressey et al. 1993; Di Benedetto et al. 2010). Interestingly, the EPR spectrum of the same amethyst sample pulverized in acetone does not contain any signal in the magnetic field below $g = 4.28$ (Fig. 1), further supporting the interpretation that the surface Fe^{3+} species on the amethyst pulverized in air formed largely from the oxidation of Fe^{2+}. Therefore, the powder sample of amethyst prepared by pulverization in air represents an excellent analogue of mineral dust containing surface Fe^{3+} species.

SivaRamaiah et al. (2011) performed detailed powder EPR measurements of this amethyst sample to obtain various thermodynamic properties and magnetic susceptibility of the surface Fe^{3+} species on quartz. In this contribution, we have conducted detailed EPR measurements of this same amethyst sample after a series of gamma-ray-irradiations (0.14–70 kGy). Specifically, new EPR spectra of the gamma-ray-irradiated sample are used to obtain thermodynamic properties (Gibbs energy, enthalpy, entropy, and activation energy), magnetic susceptibilities, relaxation times (i.e., spin–lattice relaxation time T_1 and phase memory relaxation time T_m), and the geometrical radius of the surface Fe^{3+} species on quartz. These data are compared with those from as-is amethyst (SivaRamaiah et al. 2011) to investigate the effects of gamma-ray-radiation on the surface Fe^{3+} species on quartz, with relevance to aerosol–radiation interactions.

Sample and experimental procedure

The same sample of natural amethyst investigated in SivaRamaiah et al. (2011) was used in this study to facilitate direct comparison. Powders of this sample, obtained from pulverization in air (SivaRamaiah et al. 2011), were irradiated at room temperature in a ^{60}Co cell with a dose rate of ~460 Gy/h for total doses ranging from 0.14 to 70 kGy.

All EPR spectra of the gamma-ray-irradiated amethyst and a polycrystalline $CuSO_4 \cdot 5H_2O$ standard were recorded using a Bruker EMX spectrometer equipped with a high-sensitivity ER 4119 cavity, an automatic frequency controller, and an Oxford liquid-helium cryostat, at the Saskatchewan Structural Sciences Centre, University of Saskatchewan. An empty amorphous silica tube was first recorded at room temperature (~294 K) to ensure free of any paramagnetic species. This tube was then used for recording the powder EPR spectra of the gamma-ray-irradiated amethyst and the polycrystalline $CuSO_4 \cdot 5H_2O$ standard. All experimental conditions were kept to be similar to those described in SivaRamaiah et al. (2011).

Results and discussion

The powder sample of amethyst changed from white to smoky color after gamma-ray-irradiation. The smoky coloration intensifies with increase in the radiation dose. Previous experimental and theoretical studies have shown that the smoky color of quartz is attributable to the formation of the $[AlO_4]^0$ center during irradiation (Meyer et al. 1984; Walsby et al. 2003; To et al. 2005).

EPR spectra of gamma-ray-irradiated amethyst at 294 K

Figure 2a shows that the 294 K powder EPR spectrum of 10-kGy gamma-ray-irradiated amethyst consists of three resonance signals at $g = \sim 2.00$, ~ 4.28, and ~ 15. The signal at $g = \sim 4.28$ is attributable to the substitutional Fe^{3+} ions at the Si site (Weil 1994; SivaRamaiah et al. 2011) and remains essentially constant in intensity after gamma-ray-irradiation. The signal at $g = \sim 2.00$, the well-known oxygen-vacancy electron center E_1', on the other hand, shows a minor but noticeable increase in intensity with increase in the radiation dose. Similarly, the broad peak at $g = 10.8$ (i.e., surface Fe^{3+} species; SivaRamaiah et al. 2011) shows a marked increase in intensity after gamma-ray-irradiation and shifts to a higher effective

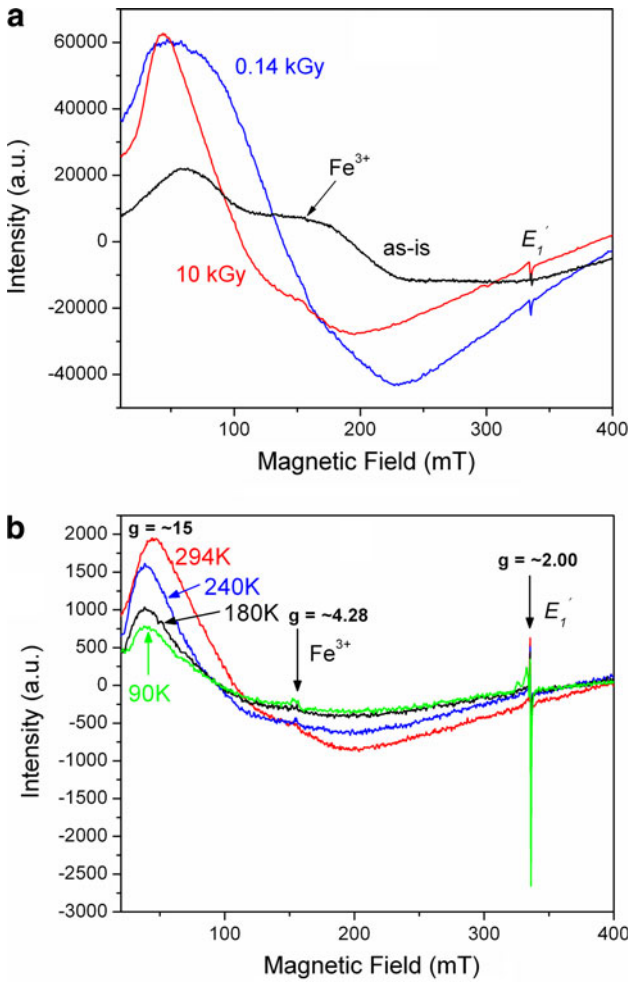

Fig. 2 Representative powder EPR spectra of gamma-ray-irradiated amethyst quartz: **a** effects of gamma-ray radiation (0.14 and 10 kGy) at 294 K, in comparison with that without irradiation (SivaRamaiah et al. 2011); and **b** at a radiation dose of 10 kGy and temperatures from 90 to 270 K

g value of ~15 (Fig. 2a). It is also interesting to note that the surface Fe^{3+} species appears to shift in the effective g value from ~14 to ~15 with the increase in the gamma-ray dose from 0.14 to 10 kGy. This shift in the effective g value toward higher values after gamma-ray-irradiation is probably attributed to interactions between the surface Fe^{3+} species and mobile electrons. Another notable feature in the EPR spectra of the surface Fe^{3+} species with increasing radiation doses is that its line shape changes from Gaussian to Lorentzian (Fig. 2a).

Free Fe^{3+} ions belong to the d^5 configuration with $^6S_{5/2}$ as the ground state, without any spin–orbit interaction. The g value of free Fe^{3+} ions is expected to lie very close to the free-electron value of 2.0023. However, the experimental g values of Fe^{3+} species in crystalline solids often deviate significantly from 2.0023, with those at ~4.28 and ~15 related to specific symmetry environments being particularly common. When Fe^{3+} ions are placed in a ligand field environment, the $^6S_{5/2}$ ground state splits into three Kramers doublets |±1/2>, |±3/2>, and |±5/2>. The resonance signal at g = ~4.28 arises from the middle Kramers doublet |±3/2> for Fe^{3+} ions in almost completely rhombic environments with the ratio of the zero-field splitting parameters |E|/|D| ≈ 1/3 (Golding et al. 1978; Pan et al. 2009). Similarly, the g = ~15 signal has been linked to Fe^{3+} ions in distorted octahedral environments as well (Sreekanth Chakradhar et al. 2005). The contrasting dependence on the radiation dose also demonstrates that the g = ~4.28 and ~15 signals in our EPR spectra (Fig. 2) belong to separate Fe^{3+} species.

EPR spectra of gamma-ray-irradiated amethyst at 90–294 K

Figure 2b shows the powder EPR spectra of gamma-ray-irradiated amethyst (10 kGy) recorded from 90 to 294 K. The broad signal at g = ~15 observed at 294 K is shifted to g = ~17 at 270 K (not shown in the Fig. 2b). This shift in the effective g value from 294 to 270 K is similar to that observed for the surface Fe^{3+} species on as-is amethyst and has been interpreted to represent a reduction in the overall paramagnetism (SivaRamaiah et al. 2011; Zhang et al. 2009). However, the effective g value at ~17 remains constant in the temperature range from 270 to 90 K (Fig. 2b).

The intensity of the g = ~4.28 signal, on the other hand, appears to be constant in the temperature range from 294 to 90 K. Therefore, this g = ~4.28 signal also differs that at g = ~15 in thermal property, further supporting our interpretation that they belong to separate Fe^{3+} species. The intensity of E_1' at g = ~2.00 decreases with increase in temperature from 90 to 294 K, which is attributable to decrease in mobile or conduction electrons when temperature is increased and is consistent with the Boltzmann law.

The resonance signal at g = ~ 15–17 decreases with decrease in temperature from 294 to 90 K, suggesting that change in the magnetic ordering is expected to be in the antiferromagnetic conditions at low temperatures. As temperature is lowered, the relaxation time increases, and the resonance peak shapes become more prominent. There is a gradual decrease in the spin moment and a loss of coherence (consistency) of spin coupling from 294 to 90 K. Also, the signal at g = ~15–17 appears to become sharper from 294 to 90 K, which is attributable to decrease in spin–spin and spin–orbit interactions and an overall decrease in the paramagnetic character (Zhang et al. 2009).

The progressive decrease in the spins, to build an antiferromagnetic (AF) structure with lowering temperature, involves the rise of the AF contribution to the EPR line, and the monotonic decrease in the number of spins is

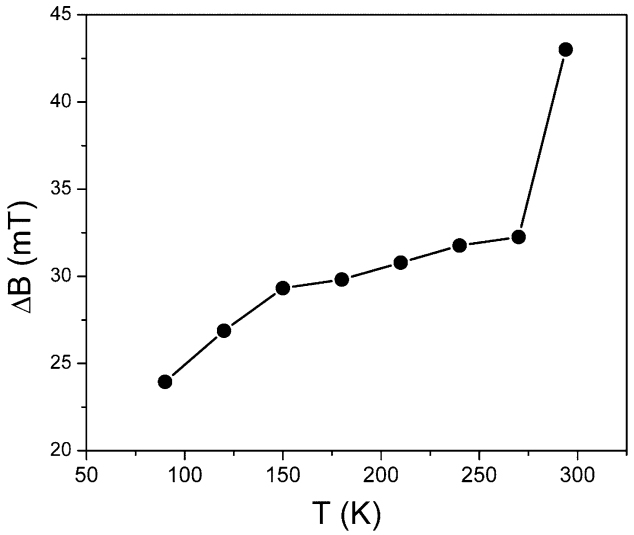

Fig. 3 Linewidth (ΔB) of the surface Fe^{3+} center on gamma-ray-irradiated (10 kGy) amethyst as a function of absolute temperature from 90 to 294 K

visible at low temperature. The occurrence of AF implies a long-range order between Fe^{3+} species. The linewidth of this signal at $g = \sim 15$–17 also decreases from 294 to 90 K (Fig. 3), which is attributable to increase in the spin–lattice relaxation time (see below). This temperature dependence of the EPR linewidth observed in the irradiated amethyst is attributable to interaction between conduction electrons and phonons (cf. Augustyniak-Jabłokow et al. 2010). This interaction leads to a temperature-dependent spin-relaxation time on the order of $\sim 10^{-8}$ s. The observed line broadening from 90 to 294 K is attributable to dipolar interactions (cf. Gaite et al. 1993).

Calculation of absolute number of spins and thermodynamic properties

The absolute number of spins (N) participating in resonance can be calculated by comparing the area under the absorption curve with that of a standard of known concentration. Weil and Bolton (2007) gave the following formula for the sample (x) and standard (std):

$$N_x = \frac{A_x(\mathrm{scan}_x)^2 G_{\mathrm{std}}(\mathrm{Bm})_{\mathrm{std}}(g_{\mathrm{std}})^2[S(S+1)]_{\mathrm{std}} N_{\mathrm{std}}}{A_{\mathrm{std}}(\mathrm{scan}_{\mathrm{std}})^2 G_x(\mathrm{Bm})_x(g_x)^2[S(S+1)]_x} \quad (1)$$

where A is the area under the absorption curve, which is obtained from double integration of the first-derivative spectrum; scan is the magnetic field corresponding to unit length of the spectrum; G is the receiver gain; Bm is the modulation amplitude; g is the g factor; S the spin of the system in its ground state ($S = 5/2$ and 1/2 for Fe^{3+} and Cu^{2+}, respectively). N_{std} denotes the number of spins in the 100 mg $CuSO_4 \cdot 5H_2O$ standard. Repeated analyses of the amethyst sample and the standard at 294 K show that the uncertainty of our calculated absolute spin number is ~ 2 %.

The absolute number of spins for the surface Fe^{3+} signal at $g = \sim 15$ in gamma-irradiated amethyst at 294 K has been found to be on the order of 10^{18} spins/g (Fig. 4a), which is comparable to those reported in the literature. SivaRamaiah et al. (2011) calculated a spin number of $\sim 4.6 \times 10^{18}$ spins/g for Fe^{3+} on the as-is quartz. Figure 4a shows that the number of spins in the gamma-ray-irradiated amethyst increases from 0.15×10^{18} to 1.21×10^{18} spins/g, when temperature increases from 90 to 294 K.

Figure 4b shows a linear relationship between $\log_{10}(N/T)$ and reciprocal of absolute temperature. This relationship allows the calculation of the entropy ΔS and the enthalpy ΔH on the basis of the intercept on the Y axis and the slope, respectively. The calculated values of entropy and enthalpy of the Fe^{3+} center in 10 kGy gamma-ray-irradiated amethyst are 0.8 (meV/K) (12.8×10^{-23} J/K) and 8.9 (meV) (14.24×10^{-22} J), respectively. These ΔS and ΔH values are notably different from their respective values of 1 meV/K and 6.29 meV for the Fe^{3+} center on

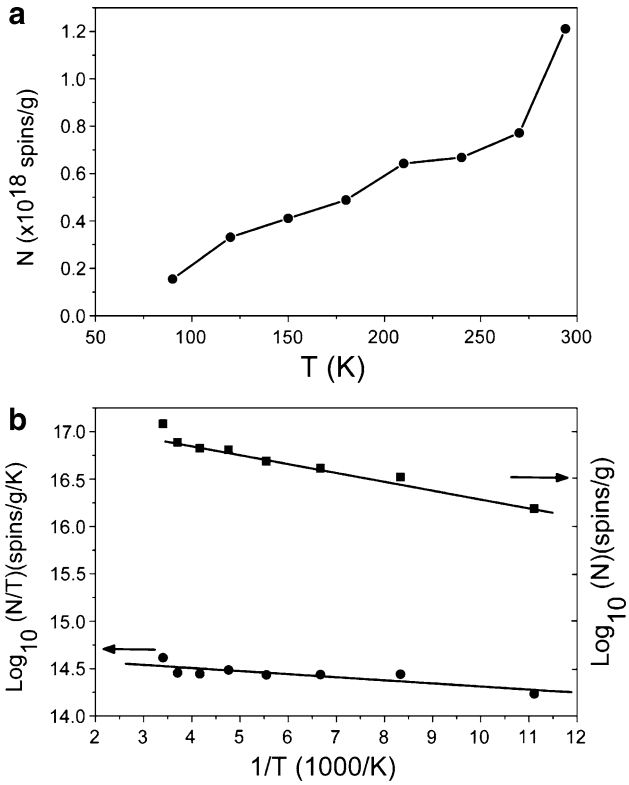

Fig. 4 **a** The number of spins (N) of the surface Fe^{3+} center on the gamma-ray-irradiated (10 kGy) amethyst as a function of absolute temperature from 90 to 294 K; **b** plots of $\log_{10}$ (N/T) and $\log_{10}$(N) versus reciprocal temperature. Note that the data point at 294 K was excluded from calculations

the as-is quartz (SivaRamaiah et al. 2011). This decrease in ΔS and increase in ΔH are attributable to both decrease in the density of mobile/conduction electrons with radiation and high exchange interaction and high strain at the field boundaries of the domains in the irradiated amethyst.

Figure 4b also shows a graph between the logarithmic number of spins and the reciprocal of absolute temperature. The slope of this graph gives the activation energy $E_a = 19.7$ meV (31.5×10^{-22} J) for the Fe^{3+} species on the gamma-ray-irradiated amethyst. The pre-exponential coefficient thus determined is 39 s^{-1}. The latter value from the gamma-ray-irradiated amethyst is similar to that for the as-is quartz (40; SivaRamaiah et al. 2011). The former value, on the other hand, is significantly larger than that (7 meV or 11.2×10^{-22} J) obtained for the Fe^{3+} species without irradiation (SivaRamaiah et al. 2011). The pre-exponential coefficient is useful for determining the spin orientation, spin concentration, and spin dynamics (SivaRamaiah and Lakshmana Rao 2012). The increase in activation energy is attributable to a decrease in the density of mobile/conduction electrons with irradiation. These results demonstrate that energy required to liberate an electron from the surface Fe^{3+} species on the gamma-ray-irradiated amethyst is greater than its counterpart without irradiation.

The Gibbs energy (ΔG) can be calculated using the equation

$$\Delta G = 2.303RT \log_{10}(k_B T/\lambda h), \quad (2)$$

where R is the universal gas constant (8.31 J/K/mol); k_B is the Boltzmann constant (1.38×10^{-23} J/K); T is absolute temperature; λ is the rate constant and is equal to the absolute number of spins per 100 mg; and h is Planks constant (6.63×10^{-34} Js). The Gibbs energy of -24.2 (kJ/mol) for the Fe^{3+} center on irradiated amethyst at 294 K is higher than the value (-27.4 kJ/mol) reported for the as-is quartz (SivaRamaiah et al. 2011). This increase in Gibbs energy by 3.2 kJ/mol after gamma-ray irradiation is an excellent line of evidence for chemical reactions involving the surface Fe^{3+} species during radiation. Such radiation-induced chemical reactions may include conversions of Fe^{3+} to Fe^{2+} and/or Fe^{4+} (Cox 1976; Dedushenko et al. 2004; Di Benedetto et al. 2010). Unfortunately, direct EPR detection of Fe^{2+} and Fe^{4+}, both paramagnetic, is not possible under the experimental condition utilized in this study.

Figure 5 shows that the Gibbs energies of the Fe^{3+} species on gamma-ray-irradiated amethyst increase with temperature, similar to that observed on the as-is quartz (SivaRamaiah et al. 2011). This temperature dependence of Gibbs energy supports strong dipolar interactions among the surface Fe^{3+} ions.

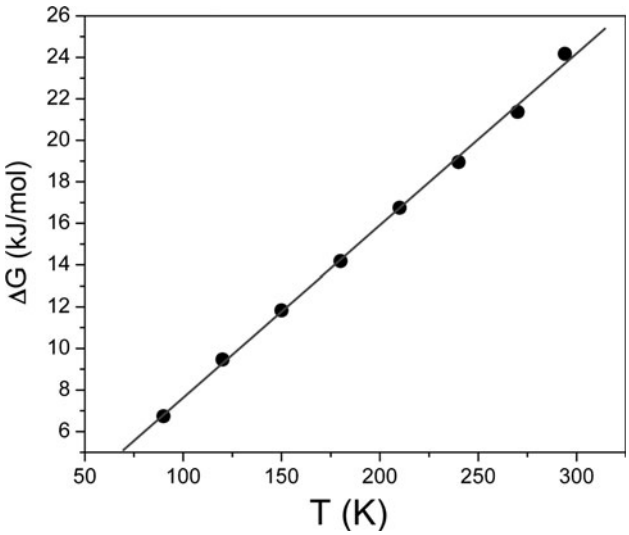

Fig. 5 Calculated Gibbs free energies (ΔG) of the surface Fe^{3+} center on the gamma-ray-irradiated (10 kGy) amethyst as a function of absolute temperature

Magnetic susceptibility

The magnetic susceptibility χ for the $g = \sim 15$–17 signal has been calculated using the equation

$$\chi = \frac{Ng^2\beta^2 S(S+1)}{3k_B T} \quad (3)$$

where N is the number of spins per m^3; g is the g factor and is equal to 15 or 17; β is the Bohr magneton (9.27×10^{-24} J/T); S is the spin quantum number of unpaired electrons = 5/2; k_B is Boltzmann constant (1.38×10^{-23} J/K), and T is absolute temperature. The magnetic susceptibilities have been calculated from 294 to 90 K. The calculated magnetic susceptibility of 1.69×10^{-2} m^3/kg at 294 K is three orders of magnitude larger than that reported by Hrouda (1986) and is also an order larger than that (3.44×10^{-3} m^3/kg) obtained from the as-is sample (SivaRamaiah et al. 2011).

Figure 6 also shows that the reciprocal magnetic susceptibility correlates linearly with absolute temperature. The intercept of this plot gives the Curie temperature of +475 K, while the reciprocal of the slope yields the Curie constant of 19.2 emu/mol. The large positive value of Curie temperature demonstrates that strong ferromagnetic interactions are present in the gamma-ray-irradiated amethyst. In comparison, the Curie temperature and the Curie constant in the as-is amethyst are only +83 K and 11.6 emu/mol, respectively (SivaRamaiah et al. 2011). These differences indicate that the surface Fe^{3+} species on the gamma-ray-irradiated amethyst has stronger ferromagnetic but weaker antiferromagnetic interactions than its counterpart on the as-is sample.

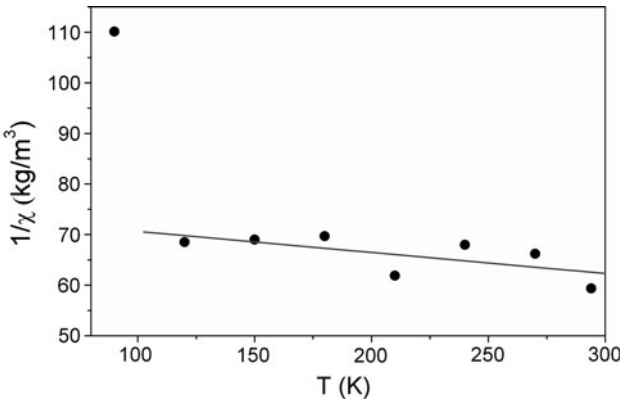

Fig. 6 Reciprocal Curie magnetic susceptibility of the surface Fe^{3+} center on gamma-ray-irradiated (10 kGy) amethyst as a function of absolute temperature. Note that the data point at 90 K was excluded from calculation

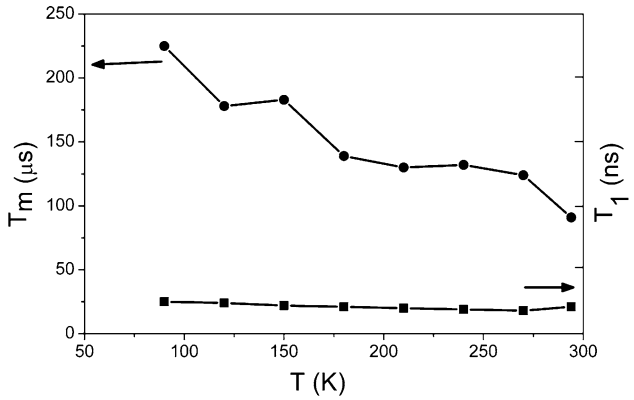

Fig. 7 Calculated phase memory time (T_m) and spin–lattice relaxation time (T_1) of the Fe^{3+} center on gamma-ray-irradiated (10 kGy) amethyst as a function of absolute temperature

Relaxation times (T_m and T_1)

The phase memory time T_m can be calculated using the equation (SivaRamaiah and Lakshmana Rao 2012)

$$T_m = 9\sqrt{3}\hbar/4\pi^2 g^2 \beta^2 N \quad (4)$$

where $\hbar = h/2\pi$; h is Planks constant; g is the g factor value of $\sim$15–17; β is Bohr magneton; and N is the number of spins in 100 mg of 10 kGy gamma-ray-irradiated amethyst. This formula deals with the absolute concentration and, therefore, is applicable for determining T_2 or T_m from both pulse EPR and CW EPR spectra. This formula yields T_m at 17.9 ns at 294 K, which is in agreement with values reported in literature (Yamanaka et al. 1996; Gubaidullin et al. 2007). For example, Yamanaka et al. (1996) reported T_m values of 18–22 ns for the E' center in the gamma-ray-irradiated quartz. Gubaidullin et al. (2007) reported a T_m value of 200 ns at the temperature range 1.6–4.2 K and noted that T_m is independent of temperature, suggesting strong dipolar interactions between paramagnetic centers in their sample. Figure 7 shows that T_m increases from 17.9 to 140 ns when the temperature decreases from 294 to 90 K. Interestingly, the calculated T_m values in the as-is amethyst are from 91 to 225 μs. It is expected that strong dipole coupling between Fe^{3+} ions results in fast relaxing with short T_m. Therefore, the calculated T_m values indicate stronger dipolar interactions among the surface Fe^{3+} ions in the gamma-ray-irradiated amethyst than those without irradiation.

The spin–lattice relaxation time T_1 can be calculated using the equation

$$T_1 \approx 2\hbar/\sqrt{3}g\beta\Delta B \quad (5)$$

where ΔB is the linewidth, $\hbar = h/2\pi$ and h is Planck's constant, $g = \sim$15–17, and β is Bohr magneton. The spin–lattice relaxation time for the Fe^{3+} species is estimated to be $\sim 10^{-8}$ s from 90 to 294 K, which is of the same order of magnitude reported by Augustyniak-Jabłokow et al. (2010). This T_1 value is four orders of magnitude larger than those (21–25 ps) for its counterpart in as-is amethyst. Figure 7 shows that T_1 decreases slightly with increasing temperature, which is attributable to spin-phonon interaction. The calculated T_1 values indicate stronger spin–lattice interactions for surface Fe^{3+} ions in gamma-ray-irradiated amethyst than its counterpart without irradiation.

Geometrical radius of surface Fe^{3+} species

The ionic radius of a transition metal ion can be calculated using the equation

$$r_t = 1/2(\pi/6N)^{1/3} \quad (6)$$

where r_t is the geometrical radius, and N is the number of spins per 100 mg. The geometrical ionic radius of the surface Fe^{3+} ions in the gamma-ray-irradiated amethyst is calculated as 9.67 μm. The geometrical ionic radius of Fe^{3+} ions in un-irradiated amethyst, on the other hand, is calculated to be 4.99 nm only. Therefore, the geometrical ionic radius of the surface Fe^{3+} species on the gamma-ray-irradiated amethyst is nearly three orders of magnitude larger than those on the as-is sample. The geometrical ionic radius can be calculated for any material where the absolute number of spins is known.

Implications for aerosol–radiation interactions

EPR studies of carbonaceous radicals in soot from incomplete combustion of fossil fuels and biomass have been shown to provide important information about the source, speciation, concentration, formation condition, and chemisorption properties of aerosols in the atmosphere

(e.g., Dzuba et al. 1988; Yordanov et al. 1996; Yordanov and Najdenova 2004; Ledoux et al. 2002; Saathoff et al. 2003; Yamanaka et al. 2005; Xie et al. 2007). Similarly, other paramagnetic species (e.g., transition metal ions such as Mn^{2+} and Fe^{3+}) in natural and anthroprogenic aerosols have been investigated by the EPR technique as well (Ledoux et al. 2002, 2004). For example, Ledoux et al. (2002) investigated the evolution of Mn^{2+} and Fe^{3+} ions in the atmospheric particulate aerosols emitted from a ferromanganese metallurgy plant near Wimereux, France.

Interestingly, the EPR spectra of their fine-grained aerosols (<1 μm; see Fig. 7 in Ledoux et al. 2002) contain a broad peak in the low magnetic field, which was interpreted to arise from a ferromagnetic phase containing Mn (cf. Petrakovskii et al. 1983). Our results from amethyst quartz offer an alternative explanation for this broad peak in the low magnetic field (i.e., ferromagnetic surface Fe^{3+} species on fine-grained aerosol particulates). One possible way for distinguishing Fe^{3+} from Mn is measuring the temperature dependence of linewidth. Figure 3 shows that the Fe^{3+} center has the observed linewidth reduced from ~45 mT at 294 K to <25 mT at 90 K. On the other hand, the linewidth of a Mn signal, with contributions from its ^{55}Mn hyperfine structure, is unlikely to go below 40 mT. Moreover, our results suggest that surface Fe^{3+} species on aerosol particulates are affected significantly by interactions with cosmic radiations and potentially exert important effects on the atmospheric cloud formation and ultimately the global climate changes.

First of all, the experimental studies (Svensmark et al. 2007; Enghoff et al. 2008, 2011) have shown that cosmic rays are active in producing small thermodynamically stable clusters, which are important for aerosol nucleation processes and cloud formation in the atmosphere. For example, Enghoff et al. (2011) demonstrated sulfuric acid aerosol nucleation in an atmospheric pressure reaction chamber by using both a 580-MeV electron beam and a 33.5-MBq Na-22 gamma source and showed that the nature of ionizing particles is not important in the radiation-induced aerosol nucleation processes. Our calculated relaxation times show that surface Fe^{3+} ions on quartz have stronger dipolar interactions after gamma-ray irradiation, which are strong evidence for radiation-induced clustering of the surface Fe^{3+} ions. Moreover, our calculated Gibbs and activation energies for the surface Fe^{3+} ions suggest that heterogeneous nucleation (i.e., those promoted by surface defects) is potentially important in radiation-induced aerosol nucleation.

Secondly, most inorganic aerosols do not absorb solar radiation but produce a negative radiative forcing by scattering incoming solar radiation back into space (Saathoff et al. 2003). Also, the radiative properties, including scattering and extinction coefficients, of aerosols are known to be sensitive to their chemical compositions and grain sizes (Tang 1996; Yu and Zhang 2011). For example, Yu and Zhang (2011) showed that the scattering and extinction coefficients increase with the geometrical radius of aerosols. Our data show that the geometric radius of the surface Fe^{3+} species increases dramatically with radiation. Therefore, interactions between aerosols and cosmic radiations may be a significant contributor to the radiative forcing of climate change.

Finally, the Fe^{3+} catalyzed oxidation of SO_2 to SO_4^{2-} in the tropospheric clouds has long been suggested to be a major contributor to acid rain (Conklin and Hoffmann 1988; Martin et al. 1991). Our thermodynamic data for the surface Fe^{3+} species on quartz before and after gamma-ray irradiation show that energy required to liberate an electron from the former is greater than the latter. This result suggests that cosmic radiation may have a negative impact on the catalytic property of Fe^{3+} in the oxidation processes in the tropospheric clouds.

Conclusions

This presentation of EPR spectra provides evidence for significant effects of gamma-ray-radiation on the surface Fe^{3+} species on quartz. In particular, the EPR spectra of the surface Fe^{3+} species on quartz before and after gamma-ray-irradiation not only differ in the effective g value but change in the observed line shape from Gaussian to Lorentzian. Also, the thermodynamic properties, the magnetic susceptibilities, the relaxation times, and the geometric radius of the surface Fe^{3+} species on quartz are affected by gamma-ray-radiation as well. These results provide compelling evidence for radiation-induced clustering of the surface Fe^{3+} ions, with relevance to the atmospheric cloud formation and precipitation.

Acknowledgments We thank Dr. Milan Rieder for his suggestion of the experiments reported in Fig. 1, which was the impetus to this study. We also thank Dr. F. Di Benedetto and an anonymous reviewer for incisive criticisms and helpful suggestions, Drs. Kuppala V Narasimhulu and J. Lakshmana Rao for discussions, and the Natural Science and Engineering Research Council (NSERC) of Canada for financial support.

References

Andreae MO, Rosenfeld D (2008) Aerosol-cloud-precipitation interactions. Part 1: the nature and sources of cloud-active aerosols. Earth Sci Rev 89:13–41

Augustyniak-Jabłokow MA, Yablokov YV, Andrzejewski B, Kempiński W, Łoś Sz, Tadyszak K, Yablokov MY, Zhikharev VA (2010) EPR and magnetism of the nanostructured natural carbonaceous material shungite. Phys Chem Minerals 37:237–247

Balitsky VS, Machina IB, Marin AA, Shigley JE, Rossman GR, Lu T (2000) Industrial growth, morphology and some properties of bi-colored amethyst citrine quartz(ametrine). J Crystal Growth 212:255–260

Barry TI, Moore WJ (1964) Amethyst: Optical properties and paramagnetic resonance. Science 144:289–290

Buseck PR, Pósfai M (2010) Nature and climate effects of individual tropospheric aerosol particles. Annu Rev Earth Planet Sci 38:17–43

Claquin T, Schulz M, Balkanski YJ (1999) Modeling the mineralogy of atmospheric dust sources. J Geophys Res 104:243–256

Conklin MH, Hoffmann MR (1988) Metal ion-sulfur(IV) chemistry. 3. Thermodynamics and kinetics of transient iron(III)-sulfur(IV) complexes. Environ Sci Tech 22:899–907

Cox RT (1976) EPR of an S = 2 centre in amethyst quartz and its possible identification as the d^4 ion Fe^{4+}. J Phys C: Solid State Phys 9:3355–3361

Cressey G, Henderson CMB, van der Laan G (1993) Use of L-edge X-ray absorption spectroscopy to characterize multiple valence states of 3d transition metals; a new probe for mineralogical and geochemical research. Phys Chem Minerals 20:111–119

Dedushenko SK, Makhina IB, Marin AA, Mukhanov VA, Perfiliev YD (2004) What oxidation state of iron determines the amethyst colour? Hyperfine Interact 156:417–422

Di Benedetto F, Innocenti M, Tesi S, Romanelli M, D'Acapito F, Fornaciai G, Montegrossi G, Pardi LA (2010) A Fe K-edge XAS study of amethyst. Phys Chem Minerals 37:283–289

Dzuba SA, Puskin SG, Tsvetkov YN (1988) Application of EPR for investigation of atmospheric aerosols. Doklady AN USSR 299:1150

Enghoff MB, Pedersen JOP, Bondo T, Johnson MS, Paling SM, Svensmark H (2008) Evidence for the role of ions in aerosol nucleation. J Phys Chem A112:10305–10309

Enghoff MB, Pedersen JOP, Uggerhøj UI, Paling SM, Svensmark H (2011) Aerosol nucleation induced by a high energy particle beam. Geophys Res Lett 38:L09805

Gaite JM, Ermakoff P, Muller JP (1993) Characterization and origin of two Fe^{3+} EPR spectra in kaolinite. Phys Chem Minerals 20:242–247

Golding RM, Singhasuwich T, Tennant WC (1978) An analysis of conditions for an isotropic g-tensor in high-spin d^5 systems. Mol Phys 34:1343–1350

Gubaidullin RR, Orlinskii SB, Rakhmatullin RM, Sen S (2007) Spectroscopic study of the effect of N and F codoping on the spatial distribution of Er^{3+} dopant ions in vitreous SiO_2. J Appl Phys 101:063529

Halliburton LE, Hantehzadeh MR, Minge J, Mombourquette MJ, Weil JA (1989) EPR study of Fe^{3+} in alpha quartz: a reexamination of the lithium-compensated center. Phys Rev B40:2076–2081

Hrouda F (1986) The effect of quartz on the magnetic anisotropy of quartzite. Studia Geophys Geodaet 30:39–45

Ledoux F, Zhilinskaya E, Bouhsina S, Courcot L, Bertho ML, Aboukaïs A, Puskaric E (2002) EPR investigations of Mn2+, Fe3+ ions and carbonaceous radicals in atmospheric particulate aerosols during their transport over the eastern coast of the English Channel. Atmo Environ 36:939–947

Ledoux F, Zhilinskaya E, Courcot L, Aboukaïs A, Puskaric E (2004) EPR investigation of iron in size segregated atmospheric aerosols collected at Dunnkerque, Northern France. Atmos Environ 38:1201–1210

Lohmann U, Feichter J (2005) Global indirect aerosol effects, a review. Atmos Chem Phys 5:715–737

Martin LR, Hill MW, Tai AF, Good TW (1991) The iron catalyzed oxidation of sulfur(IV) in aqueous solution: differing effects of organics at high and low pH. J Geophys Res 96:3085–3097

Matarrese LM, Weil JA, Peterson RL (1969) EPR spectrum of Fe^{3+} in synthetic brown quartz. J Chem Phys 50:2350–2360

Meyer BK, Lohse F, Spaeth JM, Weil JA (1984) Optically detected magnetic resonance of the $[AlO_4]^0$ centre in crystalline quartz. J Phys C: Solid State Phys 17:L31–L36

Ming J, Mombourquette MJ, Weil JA (1990) EPR study of Fe^{3+} in α- quartz: the sodium compensated center. Phys Rev B 42:33–36

Minge J, Weil JA, McGavin DG (1989) EPR study of Fe^{3+} in α-quartz: characterization of a new type of cation-compensated center. Phys Rev B 40:6490–6498

Mombourquette MJ, Tennant WC, Weil JA (1986) EPR study of Fe^{3+} in α-quartz: a reexamination of the so-called I center. J Chem Phys 86:68–79

Pan Y, Mao M, Lin J (2009) Single-crystal EPR study of Fe^{3+} and VO^{2+} in prehnite from the Jeffrey mine, Asbestos, Quebec. Canad Mineral 47:933–945

Petrakovskii GA, Piskorskii VP, Sosnin VM, Kosobudskii ID (1983) Electron spin resonance of superparamagnetic transition metal particles in polymer matrices. Soviet Phys Solid State 25:1876–1879

Saathoff H, Moehler O, Schurath U, Kamm S, Dippel B, Mihelcic D (2003) The AIDA soot aerosol characterization campaign 1999. J Aerosol Sci 34:1277–1296

SivaRamaiah G, Lakshmana Rao J (2012) Thermal and magnetic properties of VO^{2+} and Cr^{3+} centers in alkali lead borotellurite glasses. Proc Indian Nat Sci Acad 78:1–7

SivaRamaiah G, Lin J, Pan Y (2011) Electron paramagnetic resonance spectroscopy of Fe^{3+} ions in amethyst: thermodynamic potentials and magnetic susceptibility. Phys Chem Minerals 38:159–167

Sreekanth Chakradhar RP, Sivaramaiah G, Lakshmana Rao J, Gopal NO (2005) Fe^{3+} ions in alkali lead tetraborate glasses—an electron paramagnetic resonance and optical study. Spectrochim Acta, Part A 62:51–57

Svensmark H, Pedersen JOP, Marsh ND, Enghoff MB, Uggerhøj UL (2007) Experimental evidence for the role of ions in particle nucleation under atmospheric conditions. Proc Roy Soc A 463:385–396

Tang IN (1996) Chemical and size effects of hygroscopic aerosols on light scattering coefficients. J Geophys Res 101:19245–19250

Tatarov B, Sugimoto N (2005) Estimation of quartz concentrations in the tropospheric mineral aerosols using combined Raman and high-spectral-resolution lidars. Optics Lett 30:3407–3409

To J, Sokol AA, French SA, Kaltsoyannis N, Catlow CRA (2005) Hole localization in $[AlO_4]^0$ defects in silica materials. J Chem Phys 122:144704

Walsby CJ, Lees NS, Claridge RFC, Weil JA (2003) The magnetic properties of oxygen-hole aluminum centres in crystalline SiO_2. VI: A Stable AlO_4/Li centre. Can J Phys 81:583–598

Weil JA (1994) EPR of iron centres in silicon dioxide. Appl Magn Reson 6:1–16

Weil JA, Bolton JR (2007) Electron paramagnetic resonance: elementary theory and practical applications. Wiley, New York

Xie ZQ, Blum JD, Utsunomiya S, Ewing RC, Wang XM, Sun LG (2007) Summertime carbonaceous aerosols collected in the marine boundary layer of the Arctic Ocean. J Geophys Res 112:D02306

Yamanaka C, Kohno H, Ikeya M (1996) Pulsed ESR measurements of oxygen deficient type centers in various quartz. Appl Radiat Isot 47:1573–1577

Yamanaka C, Matsuda T, Ikeya M (2005) Electron spin resonance of particulate soot samples from automobiles to help environmental studies. Appl Radiat Isot 62:307–311

Yordanov ND, Najdenova I (2004) Selective estimation of soot in home dust by EPR spectrometry, Spectrochim. Acta A Mol Biomol Spectr 60:1367–1370

Yordanov ND, Veleva B, Christov R (1996) EPR study of aerosols with carbonaceous products in the urban air. Appl Magn Reson 10:439–445

Yu SC, Zhang Y (2011) An examination of the effects of aerosol chemical composition and size on radiative properties of multi-component aerosols. Atmo Climate Sci 1:19–32

Zhang SJ, Wang XC, Sammynaiken R, Tse JS, Yang LX, Li Z, Liu QQ, Desgreniers S, Yao Y, Liu HZ, Jin CQ (2009) Effect of pressure on the iron arsenide super conductor Li_xFeAs ($x = 0.8, 1.0, 1.1$) Phys Rev B 80:014506